DOI: https://doi.org/10.3986/ac.v54i2.14015

FORMATION OF CLASTIC SEDIMENTS IN THE ATL CAVE OF THE SIERRA ZONGOLICA, VERACRUZ MEXICO, AND THEIR RELATIONSHIP TO THE SOIL COVER

NASTANEK KLASTIČNIH SEDIMENTOV V JAMI ATL V GOROVJU SIERRA ZONGOLICA, VERACRUZ, MEHIKA, IN NJIHOVA POVEZAVA S POKRITOSTJO TAL

Pamela GARCÍA-RAMÍREZ[1]*, Rafael LÓPEZ-MARTÍNEZ[2], Sergey SEDOV[3], Hugo SALGADO-GARRIDO[4], Teresa PI PUIG[5] & Héctor Víctor CABADAS-BÁEZ[6]

Abstract UDC 551.442:551.3.051(23)(720.64)

Pamela García-Ramírez, Rafael López-Martínez, Sergey Sedov, Hugo Salgado-Garrido, Teresa Pi Puig & Héctor Víctor Cabadas-Báez: Formation of clastic sediments in the Atl cave of the Sierra Zongolica, Veracruz Mexico, and their relationship to the soil cover

Allochthonous cave sediments contain important paleontological and archaeological records as well as indicators of recent ecological processes. Correct interpretation of these records requires knowledge about the sediment sources and deposition processes, in particular the interrelation of vertical and lateral sediment transport. Compared to platform karst, knowledge about tropical mountainous karstic geosystems is quite limited. To trace the origin and transportation pathways of sediments, we investigated Atl Cave in the Sierra Zongolica Mountain range, Veracruz, Mexico. Field exploration and mapping have shown that the cave presents two horizontal stages representing phreatic conduits and ancient stability stages and is an epigenetic cave with a point recharge zone at the entrance, which is fed by a stream. A comparative study of the surface soil profiles and the diamicton facies of the cave floor deposits included field morphological description, micromorphological observations, grainsize analysis, colo-

Izvleček UDK 551.442:551.3.051(23)(720.64)

Pamela García-Ramírez, Rafael López-Martínez, Sergey Sedov, Hugo Salgado-Garrido, Teresa Pi Puig & Héctor Víctor Cabadas-Báez: Nastanek klastičnih sedimentov v jami Atl v gorovju Sierra Zongolica, Veracruz, Mehika, in njihova povezava s pokritostjo tal

Alohtoni jamski sedimenti vsebujejo pomembne paleontološke in arheološke zapise ter kazalnike nedavnih ekoloških procesov. Za pravilno razlago teh zapisov je treba poznati vire sedimentov in procese odlaganja, zlasti medsebojno povezanost vertikalnega in lateralnega prenosa sedimentov. V primerjavi z nižinskim krasom je znanje o tropskih gorskih kraških geosistemih precej skromno. Da bi izsledili izvor in poti prenosa sedimentov, so avtorji raziskali jamo Atl v gorovju Sierra Zongolica v Veracruzu v Mehiki. Na podlagi terenskih raziskav in kartiranja so ugotovili, da ima jama dve horizontalni stopnji, ki predstavljata freatične kanale in starodavne stopnje stabilnosti, ter da je na vhodu epigenetska jama s točko napajanja, njen vir pa je potok. Primerjalna študija profilov površinske prsti in diamiktitnega faciesa usedlin na jamskem dnu je vključevala terenski morfološki opis, mikromorfološka opazovanja, analizo velikosti delcev, kolorimetrijo, analizo kemične sestave z XRF in identifikacijo glinenih mineralov z XRD. Iz rezultatov je razvidno,

[1] Posgrado en Ciencias de la Tierra, Instituto de Geología, Universidad Nacional Autónoma de México (UNAM), CDMX, México
[2] Departamento de Dinámica Terrestre Superficial, Instituto de Geología, Universidad Nacional Autónoma de México (UNAM), CDMX, México; e-mail: rafaelopez83@hotmail.com
[3] Departamento de Ciencias Ambientales y del Suelo, Instituto de Geología, Universidad Nacional Autónoma de México (UNAM), CDMX, México; e-mail: serg_sedov@yahoo.com
[4] Instituto de Investigación Científica y Estudios Avanzados Chicxulub (IICEAC), Yucatán, México; hugoe1617@gmail.com
[5] Departamento Procesos Litosféricos and Laboratorio Nacional de Geoquímica y Mineralogía (LANGEM), Instituto de Geología, Universidad Nacional Autónoma de México (UNAM), CDMX, México; e-mail: tpuig@geologia.unam.mx
[6] Escuela Nacional de Conservación, Restauración y Museografía, Instituto Nacional de Antropología e Historia (INAH), CDMX, México; e-mail: victor_cabadas_b@encrym.edu.mx
* Corresponding author, e-mail: arqueopams42@outlook.com.

Received/Prejeto: 4. 12. 2024

rimetry, bulk chemical composition via XRF, and clay mineral identification by XRD. The results demonstrate that the cave deposits have more similarities with the young alluvial and colluvial soils near the entrance than with mature Terra Rossa developed over the limestone formation that hosts the cave. This proves the predominant role of the lateral alluvial transport by high energy events in the formation of the cave diamicton with very restricted contribution of the vertical erosion of Terra Rossa. The main source rock for alluvial and colluvial materials transported to the cave are siliciclastic sediments of the Necoxtla formation, whereas Terra Rossa soils were formed from tephra of the Orizaba volcano. High CIA values, high clay content with a predominance of kaolinite, point to greater weathering of Terra Rossa in comparison with other studied surface and underground materials.
Keywords: mountainous karst, Atl cave, cave sediments, sediment formation, soil cover, lateral erosion.

da so jamski nanosi bolj podobni mladim aluvialnim in koluvialnim tlom v bližini vhoda kot pa tlom Terra Rossa v zrelem stadiju, ki so se razvila nad apnenčasto formacijo, v kateri je jama. To dokazuje prevladujočo vlogo lateralnega aluvialnega prenosa z visokointenzivnimi dogodki pri oblikovanju jamskega diamikta z zelo majhnim prispevkom vertikalne erozije tal Terra Rossa. Glavna izvorna kamnina aluvialnih in koluvialnih materialov, ki tvorijo nanose v jami, so siliciklastični sedimenti formacije Necoxtla, tla Terra Rossa pa so nastala iz tefre vulkana Orizaba. Visoke vrednosti kemijskega indeksa sprememb in visoka vsebnost gline s prevladujočim kaolinitom kažejo na večji vremenski vpliv tal Terra Rossa v primerjavi z drugimi proučenimi površinskimi in podzemnimi materiali.
Ključne besede: gorski kras, jama Atl, jamski sedimenti, nastajanje sedimentov, pokritost tal, lateralna erozija.

1. INTRODUCTION

Cave sediments have been studied under many different approaches including: 1) as a sink of contaminants useful for tracing their movement from surface to underground and to the aquifer (Lynch, et al., 2007; Mahler, et al., 2007; Loop, 2019; Vesper, 2019), 2) as a source of paleoclimate and paleoenvironmental records such as isotopes, pollen and macro-rest (Burger, 2004; Harmon et al., 2007; Knapp, et al., 2007; White, 1988 and 2004; Dreybrodt, 2012; Zupan et al., 2020), and 3) as records of anthropic activities and occupations through time, from early Paleolithic to "sacred places" of historical cultures (Ardelean et al., 2020; Béres et al., 2021).

Cave sediments have different processes of formation, origin, and type (Ford and Williams, 2007; Springer, 2012). Two major groups of components could be discriminated: sediments from outside of the cave called allogeneic, and those formed within the cave known as autogenic. Understanding of the origin and mechanisms of transportation of the allogeneic material has major importance for most cave sediment research.

Allogeneic materials can enter the cave system by vertical or lateral transport. Sedimentary structures, particle size and sorting results from the sedimentation mechanism and pathway of the sediments. Vertical transport occurs through the system of cavities generated by dissolution in the epikarst zone. It consists of the redeposition of the materials from the surface soil mantle, involving predominantly smaller particles: silt and clay; this process is also known as "soil piping" (suffusion) (White, 1988; Beck, 2012). Lateral fluvial transport can move large amounts of material of all sizes and of different origins, from soils to fluvial and aeolian sediments (Bosch and White, 2007, 2018; Springer, 2012). Both types of erosion impact the surface soil cover of the karstic geosystems. In fact, soil development on the karst surface is a product of balance between generation of soil by pedogenesis and its loss due to "hidden" vertical erosion (Sedov et al., 2023). In some cases, this balance could shift towards nearly complete degradation of the soil mantle (Atalay, 1997). Spatial variability of erosion processes results in complex composition of the soil cover on calcareous rocks which combines thin poorly developed profiles of Rendzina type and deep red soils known as *Terra Rossa*. The latter are enriched in silicate clay and iron oxides (hematite and goethite) and leached of carbonates (Yaalon, 1997; Durn, 2003; Priori et al., 2008). The genesis of *Terra Rossa* has been a matter of intense debate for decades, especially regarding the origin of the silicate components. The lithomorphic theory states that the accumulation is from the lime-free residue of the underlying calcareous rocks (e.g. Bronger and Sedov, 2003; Bautista et al., 2011), whereas the alternative explanation points to allochthonous, mostly windblown material (Yaalon, 1997; Durn et al., 1999; Priori et al., 2008; Cabadas et al., 2010). Terra Rossa are also affected by karstic erosion and there is evidence of red soils redeposited in the interior of caves (Osborn, 1992, 2001; Lynch et al., 2007; Musgrave and Webb, 2007). Thus, underground pedosediments could provide important information about the history of soil development and soil erosion on the land surface of karstic landscapes.

Calcareous rocks affected by strong karstification occupy vast areas within the tropical zone of Southern Mexico. Large parts of these areas were subjected to long-

term human occupation and hosted highly developed Prehispanic civilizations, in particular, the ancient Maya culture. The soil mantle of the south Mexican karstic landscape comprised a vital resource for Mayan agrosystems and was severely transformed by human-induced erosion and degradation (Dunning et al., 2002; Beach et al., 2006), which is reflected in the properties of the underground pedosediments (Sedov et al., 2023). The soil erosion and redeposition processes are better documented in the platform karst landscapes of the Yucatan peninsula (Sedov et al., 2008, Cabadas et al., 2010; Sedov et al., 2023). There the vertical redeposition by suffusion was proven to be a principal process of pedosediments accumulation in the karst pockets and cave floors, with

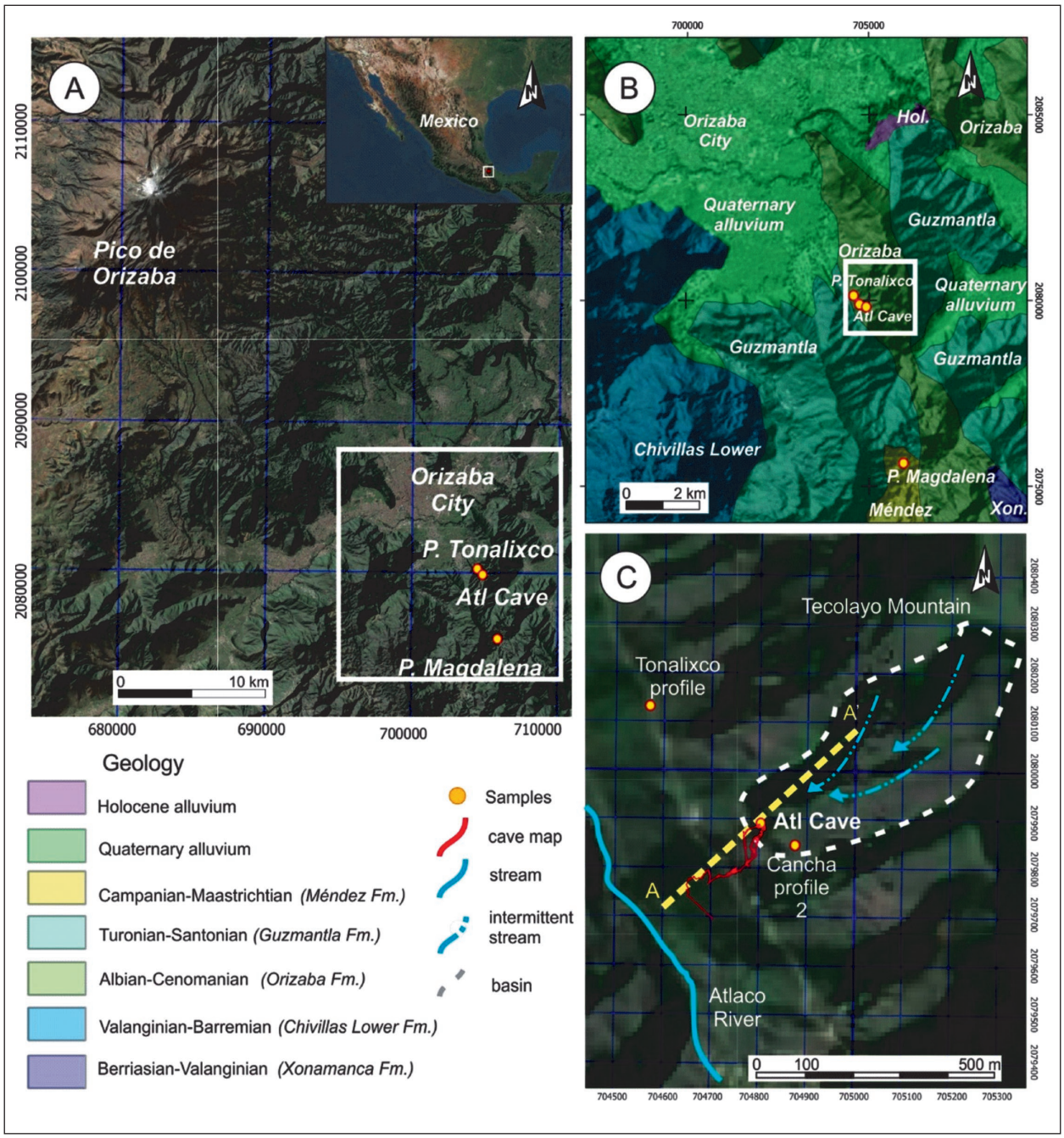

Figure 1: The study region. A) Location of Sierra Zongolica in Mexico, close to Orizaba City and the volcano Pico de Orizaba, B) Distributions of profiles in the regional geology (SGM, 2001), and C) Context of Atl cave, which is located at the bottom of a closed depression fed by three streams. This cave represents the main drainage of the small basin of 0.15 km2 with a high precipitation regime. A-A' show the cross section for Figure 2a.

minimal contribution by lateral fluvial transport. Much less is known about the processes of the underground sedimentation in the high-relief karst landscapes of the fold and thrust belt of calcareous rocks of the Chiapas and Veracruz territories.

In this research, we focus on the origin of allogeneic sediments found inside the Atl cave (Sierra Zongolica Mountain range, Veracruz state, eastern Mexico); these sediments comprise a mix of carbonate and siliceous materials in a diamicton facie at the cave bottom. Our research team, which includes soil scientists and karstologists, investigated the relationship between the soil and sediment cover on the surface around the cave and the cave floor sediments, as a way of understanding the sources of deposited materials and the pathways of their transport. We also characterized the pedogenesis of different soils formed in the karstic landscape of the Sierra Zongolica the Sierra Zongolica to better understand the interaction between the surface and underground processes.

2. MATERIALS AND METHODS

2.1 STUDY REGION

The study region is in the Sierra Zongolica, Veracruz, Mexico (Figure 1). The Sierra is part of the Maya Terrain (Ortuño et al., 1992) and is considered a prolongation of the Sierra Madre Oriental with similar tectonic behavior. The geological evolution of this zone is related to the opening of the Gulf of Mexico with complex tectonic settings and the formation of some sedimentary basins and its evolution from the late Jurassic to the late Cretaceous. During this period, a thick package of carbonate and carbonate-siliciclastic was deposited, allowing several caves to form during its exposition.

Three geological formations are involved in the development of Atl Cave. The Orizaba Formation was described by Viniegra (1965) as gray limestone divided into two main facies: Rudist boundstone and grainstone-packstone of bioclast deposited on a shallow water platform during Albian-Cenomanian. This unit is reported to be up to 2000m thick (Martínez-Amador et al., 2002).

The Maltrata Formation was described by Böse (1899) as thin stratified limestone with intercalations of slate and shale. This formation is concordant with the Orizaba Formation and it was deposited in a basin environment during the Late Cenomanian-Conacian (Arámburo-Pérez et al., 1987).

The Necoxtla Formation is still an informal unit, first described by Böse (1899) and more recently by Viniegra (1965) as a sequence of slate, shale, sandstone, and limestones with pyrite and some concretions. The age is estimated as Aptian-Albian and deposited in a basin environment with an estimated thickness up to 300m.

In this zone, Eguiluz et al., (2000) recognizes three deformation phases: laramide with shortness ENE-WSW, an extensional phase with NE-SE orientation, and the last with shortness in NW-SE direction. This deformation triggers multiple folds and fractures, favoring karst development in the area.

The Cenozoic is associated with the Transmexican-Volcanic Belt (TMVB) and represented by the Sierra Negra volcano (4585 masl) and Pico de Orizaba volcano (5670 masl), located very close to each other, sharing the same basement. The first one is an inactive stratovolcano of andesitic composition. The second is an active stratovolcano of andesitic-dacitic magma, which currently consists of a fumarole, and previously has had effusive and explosive activities (Carrasco-Nuñez and Rose, 1995; Carrasco-Nuñez, 1999).

The area presents vegetation corresponding to a High Evergreen Forest and a Mesophyll Forest of Mountain. The climate is characterized by an average annual temperature of 17.6°C; and mean annual precipitation of 2,770 mm, distributed over 196 days a year, and a total evaporation of 1,014.8 mm (CONAGUA, 2020).

2.2 SPELEOLOGICAL RESEARCH

Atl Cave takes its name from the Nahuatl term *Atl*, which means water. The cave was first explored by Benjamín Guerrero, Rodolfo Hernández, Octavio Luno and Nadia Mota González, and then by the Montañismo UNAM and Laboratorio de Carbonatos y Procesos Kársticos of UNAM. The cave was mapped following the standard mapping methods of Haüselmann (2011), with a laser distance meter and Brunton compass. The cave is still under exploration.

2.3 PEDOLOGICAL AND SEDIMENTOLOGICAL INVESTIGATION

2.3.1 Studied profiles

The selection of profiles was made to compare the sediments inside the cave, with the soil cover outside the

cave. Six profiles were studied, four outside and two inside.

The profiles on the surface include two in a doline adjacent to the cave, and two in small depressions of the limestones of the Orizaba Formation. These positions were selected because they cover the possible origins of the sediments in the cave, one by lateral and one by vertical erosion. The two profiles inside the cave were in subhorizontal passages close to 1400 masl. These profiles were selected based on thickness of the underground bottom sedimentary layer and feasibility of obtaining samples. The profiles were described in the field following the IUSS Working Group WRB (2015), and sampled for physicochemical, micromorphological and mineralogical standard analysis; the analyses were made in fractions below 2mm (sand, silt and clay).

2.3.2 Micromorphology

All soil horizons and sediment levels were sampled in undisturbed blocks from which thin sections were made and impregnated with resin Crystal MC-40 inside a vacuum chamber. When the resin was solidified the block was cut, polished and mounted on glass slides to further thin the sample until a 30 microns thin section was obtained. An Olympus model BX51 petrographic microscope was used for the study. The analysis and description were made following the terminology of Stoops (2003).

2.3.3 Physicochemical: Color and Texture

Selected physicochemical analyses were done at the Laboratory of Paleosoils of the Instituto de Geología of UNAM and at the LANGEM-IGL of UNAM.

Color. The color was determined using a Colorimeter ColorLite sph870, registering the CIEL Lab color (L*a*b*), which indicates the Lightness (L*), the Red/Geen value (a*) and Blue/Yellow (b*).

Particle size. The analysis was made following Flores and Alcalá (2010) using the pipette method. For this analysis the samples were pretreated with hydrogen peroxide (H_2O_2) to dissolve the organic matter functioning as a cementing agent, then the sample was put to agitate for 12 hours with 10 ml of sodium hexametaphosphate and 25 ml of distilled water before proceeding with the determination of the particle's percentages.

2.3.4 Mineralogical investigations by X-ray diffractometry (XRD)

XRD bulk rock and clay-oriented specimens of selected horizons of the soil and sediment profiles were made in the Laboratorio de Difracción de Rayos X, of the LANGEM-IGL, UNAM. The measurements were made with an EMPYREAN XRD diffractometer using CuKα radiation, nickel filter, and PIXcel 3D detector. The measurements were made with a step size of 0.003° (2theta) and 40s of integration time. For the analysis of the diffractograms, the software HIGHScore v4.5 was used with the ICDD (International Center for Diffraction DATA) and ICSD (Inorganic Crystal Structure Database) database.

Bulk rock samples. The samples were pulverized using an agate mortar, sieved to less than 45 microns and mounted in a back-side aluminum holder. The semi-quantification was obtained using the RIR (Reference Intensity Ratio) method (Hubbard and Snyder, 1988), implemented in the HIGHScore v4.5 software.

Oriented samples. According to Stokes' law, the clay size fraction (<2 μm) was separated by centrifugation in distilled water. Air-dried oriented preparations were obtained from the <2 μm fractions by pipetting some drops of the suspension onto a glass slide and then drying at 30°C for a few hours (Moore and Reynolds, 1997). Three aliquots were measured in air-dried form (AD), ethylene glycol saturated (EG), and heated (550°C). Clay species were estimated in semiquantitative form, using simple peak weighting factors. For area estimation we used Fityk (Wojdyr, 2010), a program for data processing and nonlinear curve fitting, simple background subtraction and easy placement of peaks and changing of peak parameters. For better evaluation of the crystallinity of the main mineral components, we measure Full Width at Half Maximum (FWHM) values. The FWHM is a key parameter in X-ray diffraction (XRD) used to evaluate the crystalline quality of minerals, particularly those belonging to the clay group. This parameter allows distinguishing between well-crystallized (low FWHM values expressed as narrow peaks) particles and those with lower structural order (high FWHM values expressed as broad peaks), while also providing insights into their formation conditions.

2.3.5 Bulk chemical composition by XRF

The analysis was made at the Laboratorio de Fluorescencia de Rayos X, at LANGEM of the Instituto de Geología. Major elements were measured in molten samples, using a Rigaka Primus II equipment, in selected horizons of the studied soil profiles. Chemical Index of Alteration (CIA) was applied to explore the weathering trends in the profiles (Nesbitt and Young, 1982); it was also used to evaluate the extent of the transformation of the feldspars group to kaolinitic clay minerals (Nesbitt and Young, 1982, 1989; Fedo et al., 1995; Maynard 1992; Price and Velbel, 2003).

3. RESULTS

3.1 CAVE DESCRIPTION OF ATL CAVE

Atl Cave (14Q 0704804E 2079891N) is in a blind valley fed by three mains streams (Figure 1c). The cave is the foremost drain system for this slight, closed depression. Its morphology presents narrow passages, scarce speleothems, and abundant allogeneic sediments. The cave exhibits a near vertical development with two horizontal stages representing phreatic conduits and ancient stability stages at 1400 and 1300 masl, the current base level of the near zone being 1248 masl (Atlaco Ravine) (Figure 2A).

So far, the cave has been mapped to 256 m of horizontal development and -120 m of depth development (Hernández-Vergara, 2017). It shows two principal galleries (Figures 2B and 2C). One of them ends in a seasonal small lake towards the north; the other goes south to Atlaco Ravine. This gallery is at the bottom of the cave; however, the gallery continues in a small and quite narrow passage.

3.2 PEDOLOGY

3.2.1 Studied profiles

The profiles studied can be divided into three groups:

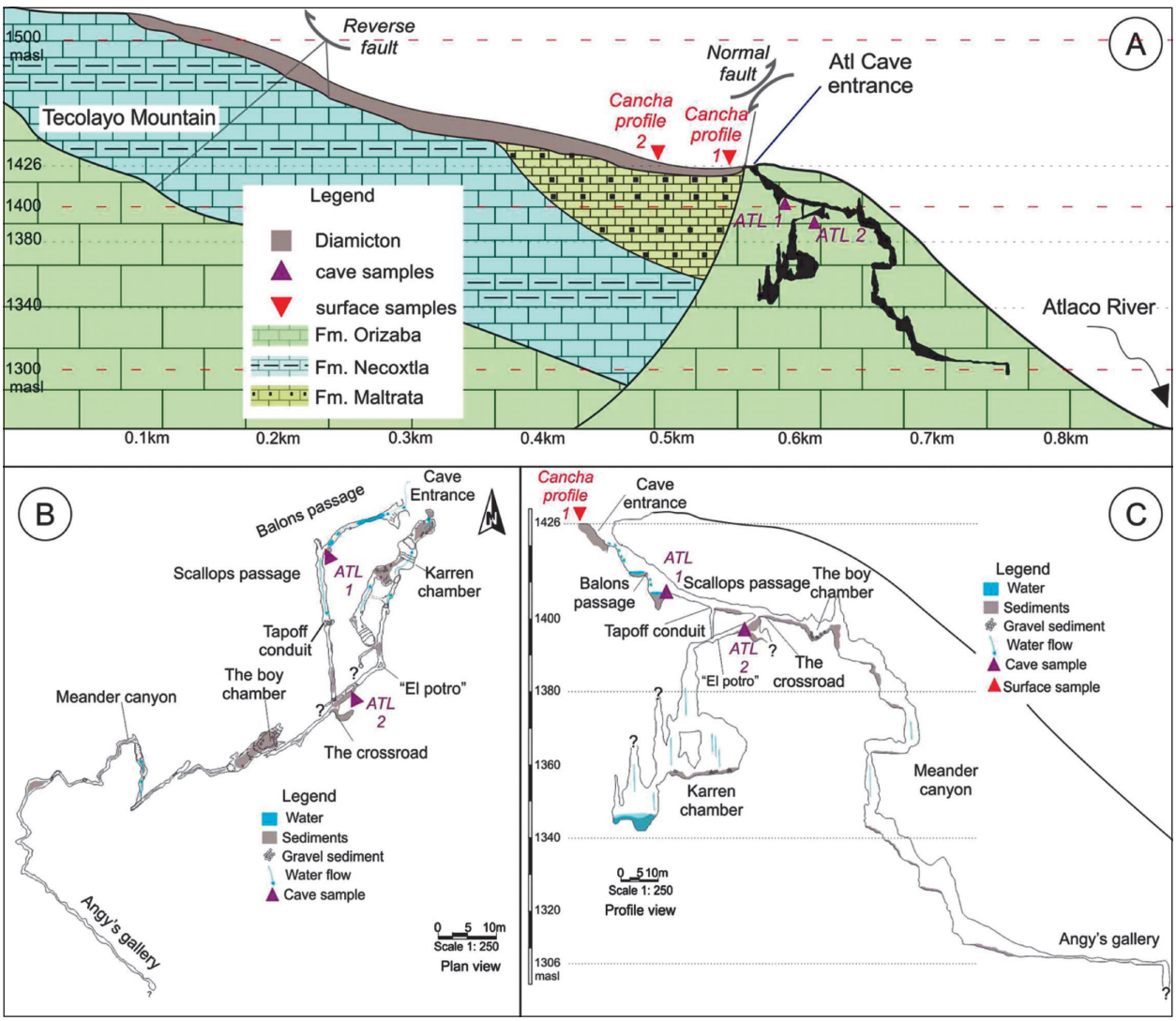

Figure 2: Section of Tecolayo Mountain and Atl cave map. A) Profile of Tecolayo Mountain and surrounding basin; B) Plan view of Atl Cave; and C) Profile view of Atl Cave (modified from Hernández-Vergara, 2017). It is possible to see how the cave collects the water of the basin and transports it into an underground drain system to the Atlaco Ravine.

Figure 3: Terra Rossa Type profiles. a) Magdalena profile; b) area of Tonalixco; and c) Tonalixco profile.

1) Terra Rossa Type. Located in small depressions in the surface landscape. Both present reddish colors and clayey texture (Figure 3 and Table 1).

- The Tonalixco profile is in the same formation as the cave Atl (14Q 0704572E 2080131N). It is an Abruptic Luvisol (Cutanic, Profondic) and has a depth of 300cm and an Ah-AB-Bw-Bt1-Bt2-BCt sequence of horizons. The topsoil shows grey-brown humus pigmentation, whereas the B horizons have a red-brown color. Evidence of clay illuviation cutans on the aggregate surfaces starts at 110 cm (Bt1 horizon) and through the rest of the profile.
- The Magdalena profile is ~5km south from the area (14Q 0705935E 2075564N). It is a Stagnic Luvisol (Clayic, Cutanic, Profondic). It has a depth of 300 cm and a Ah-Bw1-Bw2-Bg-2Bt1-2Bt2 sequence of horizons. This profile presents abrupt and strongly undulating contact with the underlying karstified limestone. In the left part of the profile where calcareous rock is closer to the surface, the specific 3Btg horizon was observed in direct contact to the limestone. Clay cutans are observable at 150 cm (2Bt1 horizon) and some redoximorphic (Stagnic) properties at the Bg and 3Btg horizon, both starting at 130 cm, but in the latter, they are combined with clay cutans.

2) Stagnosols. Located at opposite ends of a doline, adjacent to the entrance cave, that forms a somewhat flat terrain in the Sierra landscape; both profiles present colluvial materials (Figure 4 and Table 1).

- Cancha 1 profile is located at the cave entrance (14Q 0704805E 207989N), and is exposed on the bank of the stream entering the cave; the profile shows evidence of colluvial and alluvial materials. It is a Gleyic Stagnosol (Clayic, Colluvic, Skeletic), formed by an Ah-Bw1-Bw2-BCg-Cg sequence of horizons, up to 250 cm depth. High content (~50%) of weathered siliciclastic rock fragments such as siltstone and shale is observed throughout the profile starting at the Ah horizon, and redoximorphic properties are present in the BCg and Cg horizons, at 132 cm and 250 cm.
- Cancha 2 profile is located to the opposite extreme of the doline (14Q 0704877E 2079846N), at the lower part of the slope delimiting the depression presenting colluvial influence. It is a Gleyic Stagnosol (Endoskeletic) and is shallower than Cancha 1, with a depth of 100 cm and an Ah-Bg-Bw-BC sequence of

Figure 4: Stagnosols soil profiles: a) Cancha 1 profile; 2) Entrance to Atl Cave close to Cancha 1 profile; and 3) Cancha 2 profile.

Table 1: General matrix profile properties. Structure: SB: Subangular blocky, AB: Angular blocky, GR: Granular, MA: Massive, PR: Prismatic. HCl reaction: weak (X) to strong (XXX).

Horizon	Depth (cm)	Color (dry)	Structure	Texture	HCl	Others
Tonalixco						
Ah	0-30	7.5YR 3/4	GR	Silt Loam	-	Organic detritus, gradual limit.
AB	30-60	7.5YR 3/4	SB to GR	Loam	-	Low density, gradual limit.
Bw	60-110	7.5YR 4/6	SB	Clay	-	Compact, biogenetic pores, gradual limit.
Bt1	110-170	7.5YR 4/6	SB	Clay	-	Compact, wavy limit.
Bt2	170-210	7.5YR 5/6	SB	Clay	-	Similar to the previous but less red.
BCt	210-300	7.5YR 4/6	SB	Clay	-	Interior of soil aggregates of yellow color. Compact.
Magdalena						
Ah	0-40	7.5YR 3/3	GR to SB	Silty Clay Loam	-	Clear limit.
Bw1	40-100	10YR 6/6	SB	Clay	-	Fine porosity. Thin cutans and gradual limit
Bw2	100-130	10YR 5/6	SB	Clay Loam	-	Gradual limit.
Bg	130-150	10YR 6/6	SB	Clay	-	Incline clear limit.
2Bt1	150-210	7.5YR 5/6	SB	Clay	-	Low fine porosity, compact, cutans.
2Bt2	210-300	7.5YR 5/6	SB	Clay	-	Similar to the previous but less red, more compact and with cutans.
3Btg	Bg to 2Bt2	7.5YR 4/6	SB to PR	Clay	-	Located at the left side of the profile, in contact with the limestone outcrop. Fe-Mn concretions, rounded of 2mm.
Cancha 1						
Ah	0-25	10YR 6/4	GR	Silty Clay	-	Angular fragments of weathered stone without clear orientation.
Bw1	25-75	10YR 6/4	SB	Silty Clay	-	Rock fragments with green and pinkish mottling. 50% presence of gravels and stones.
Bw2	75-132	10YR 7/4	SB	Silty Clay Loam	-	Similar to the previous one. Clear limit.
BCg	132-190	10YR 7/6	-	Silty Clay	-	Mottling color (brown, green-gray, pink and yellow). Manganese presence. 60% pedegrosity.
Cg	190-250	10YR 7/4	-	Silty Clay	X	70% pedegrosity. mottling and coatings of Mn. Gray-green siltstone rock.
Cancha 2						
Ah	0-20	10YR 6/3	GR to SB	Silty Clay	-	Wavy clear limit.
Bg	20-40	10YR 7/4	SB	Silt Loam	-	Mottling of Mn and Fe, gravel and weathered rock fragments as inclusions (30%). Gradual limit.
Bw	40-70	10YR 7/4	SB	Silty Clay Loam	-	Reddish mottled given by lithics (40%). Gradual limit.
BC	70-110	10YR 7/6	SB	Silty Clay	-	Weathered siltstone rock of gray color in more than 50% of the horizon.
Atl 1						
Level 1	0-20	10YR 7/6	MA	Silty Clay	XXX	Composed of unsorted sub-angular to cobble small clast (~5-10 cm).
Atl 2						
Level 1	0-	7.5YR 7/6	MA	Clay Loam	XXX	The sediment size was between 5-10 cm.
Level 2	70-	7.5YR 6/6	MA	Clay Loam	XXX	Size clasts of ~10-15 cm.
Level 3	200-	7.5YR 7/4	MA	Clay Loam	XXX	Composed of sub angular clast of at least 20 cm.

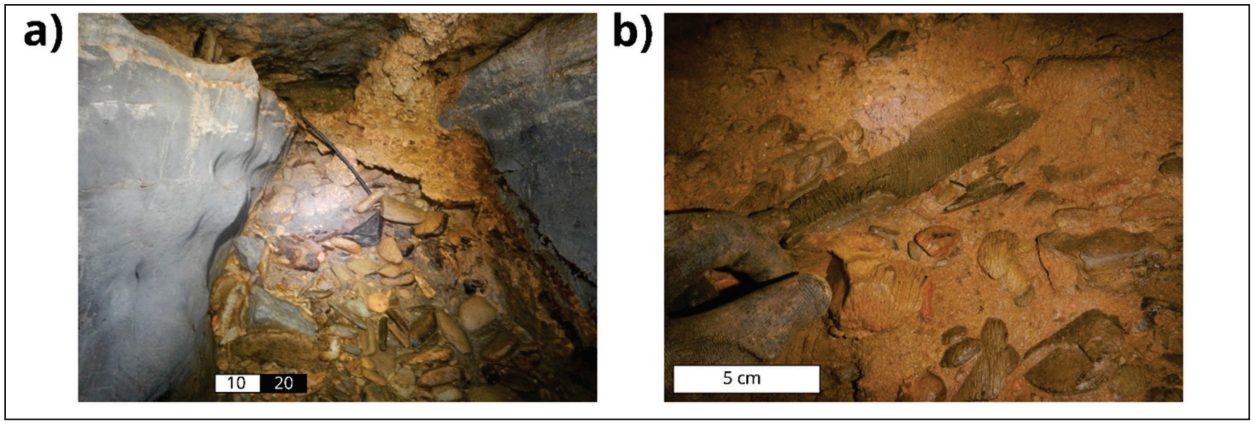

Figure 5: Diamicton profiles. a) Diamicton deposit inside the cave; and b) Close up to the diamicton deposit.

horizons. It has weathered rock fragments (~40%) starting at the Bg horizon, 20 cm, and some redoximorphic properties in the same horizon with the presence of Mn and Fe mottles.

3) Diamicton. Located in passages of the cave, both profiles are classified as diamicton facies, and are close to 1400 masl, at -30m depth from the cave entrance with a different horizontal distance (Figure 2B, 5 and Table 1)

- Atl 1 profile is located 30 m horizontally from the cave entrance at the end of "Ballons passage." Its thickness is 20 cm. The profile is composed of a brownish, massive unconsolidated matrix-supported deposit.
- Atl 2 profile is located 70 m horizontally from the cave entrance at "The crossroad" passage. Its thickness is 2m. This profile exhibits a brownish, massive unconsolidated, matrix-supported deposit, but shows a wider range of unsorted particle sizes. The profile was sampled at 0 cm, 70 cm, and 200 cm in depth.

3.2.2 Micromorphology

The Terra Rossa Type profiles present complex structure in the upper humus horizons. Small granular aggregates are clustered in the larger porous rounded blocks (Figure 6a). These horizons present fine clayey groundmass with organic pigment incorporating inclusions of charcoal fragments, clay papules and reddish soil fragments (Figure 6b), as well as some volcanic minerals: pyroxene and plagioclase. Below, in the B horizons, these soils present a homogeneous fine clay matrix with reddish ferruginous pigment (Figure 6c), with subangular blocky structure.

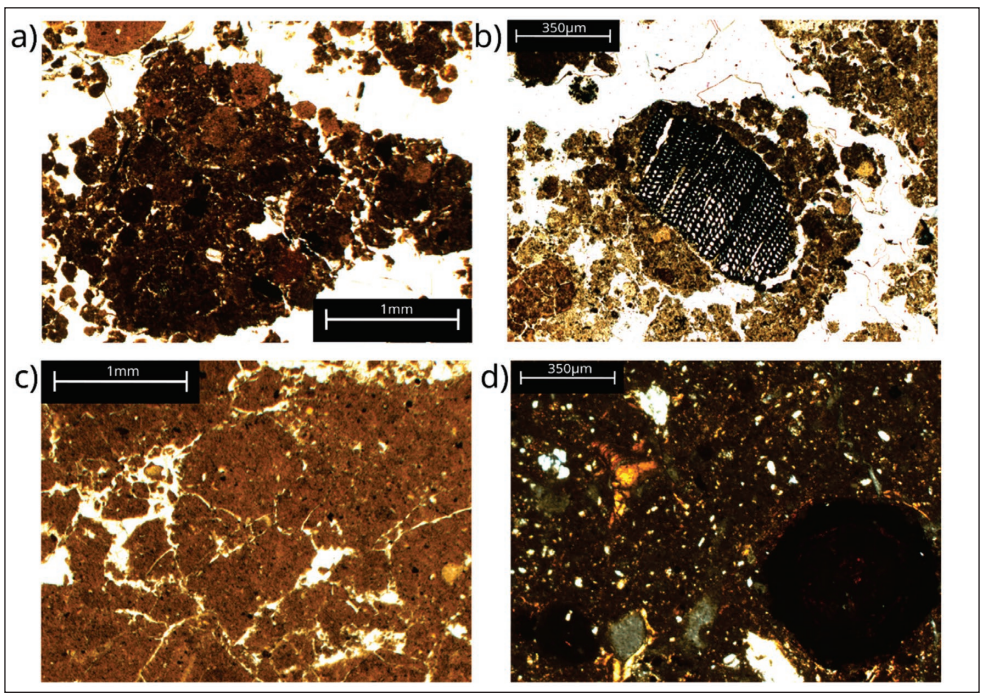

Figure 6: Micromorphology from the Terra Rossa type profiles: a) Magdalena-Ah. Matrix with granular aggregates PPL; b) Tonalixco-AB. Charcoal fragment, granular structure and clay papules PPL; c) Tonalixco-Bt1. Matrix with clay accumulation PPL; and d) Magdalena-3Bt. Clay and iron nodules NX. PPL: plane polarized light, NX crossed polarizers.

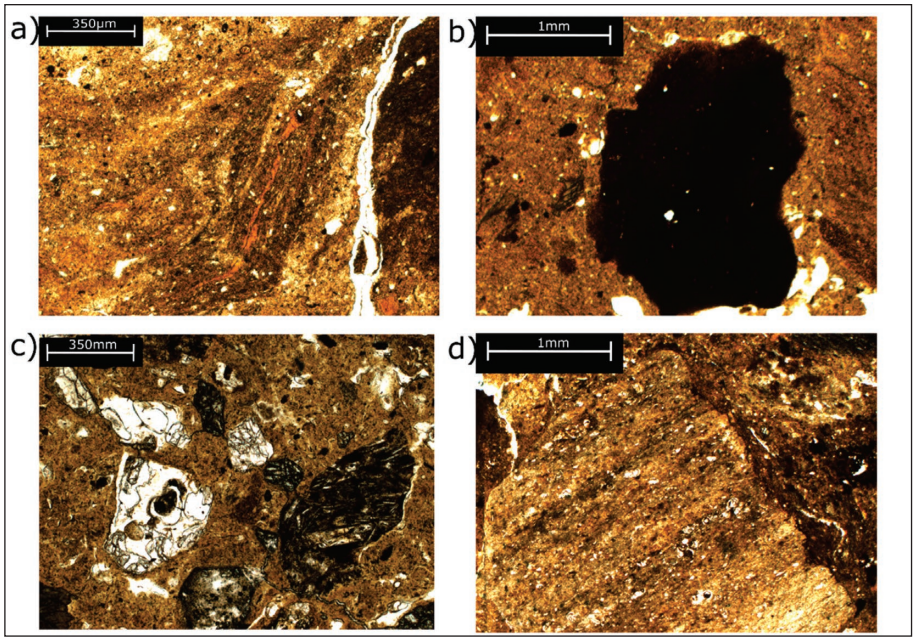

Figure 7: Micromorphology of the Stagnosols profiles. a) Cancha 1-BCg rock fragment and fluvial structure with clay cutans NX; b) Cancha 2-Bg. Clay illuviation and Fe precipitations NX; c) Cancha 1-Bw1. Sandy matrix with presence of volcanic rock fragments and minerals PPL; and d) Cancha 1-BCg. Rock fragment (shale) PPL. PPL: plane polarized light, NX crossed polarizers.

In some horizons, we observed small illuvial clay coatings, ferruginous rounded nodules (Figure 6d) and a few charcoal fragments.

In contrast, the Stagnosols profiles don't present a well-developed microaggregation in the A horizons. In general, pedogenetic features are less developed and sedimentary structures still visible, in particular microlamination and fluidal structure of fluvial origin in the profile Cancha 1 (Figure 7a). Pedofeatures include Fe-Mn nodules indicative of redoximorphic process (Figure 7b). These soils contain abundant inclusions of rock fragments (~50%) mainly shales (Figure 7d) and siltstone. Soil groundmass shows areas of sandy texture due to the presence of volcanic rocks and minerals (Figure 7c) which alternate with the areas of finer texture with materials derived from the disintegrated shales.

The Diamicton profiles are somewhat like the previous group, they present high proportions of big rock fragments (30-50%) in a fine brown matrix, with some groundmass of lighter color and texture (Figure 8a), and in some areas the matrix shows evidence of fluvial deposition with fluidal structures (Figure 8b).

3.2.3 Physicochemical: Color and Texture

Color. Colorimetric analysis shows two groups in the Luminosity values (L*), the dark colors (~60 to 40) and the light colors (~60 to 70); the first ones correspond to the Terra Rosa Type profiles and the second ones to the Stagnosols and Inside Cave profiles. The a* values present slightly higher values in the Terra Rosa Type and Inside Cave groups, while the b* values are higher for the Stagnosols and Diamicton profiles than to the Terra Rosa Type group where they are closer to the a* values (Figure 9).

Texture. In general, the texture shows a predominance of silt and clay particles. The Atl 2 profile and some horizons of the Tonalixco profile show higher values of sand content but not as the predominant component (Figure 9).

The Terra Rosa Type profiles present predominantly clayey textures. The Magdalena profile presents higher percentages of clay in the lower horizons and the silt percentage is bigger in the upper horizons. The Tonalixco profile presents three clear sections, in the first the silt predominates, the second shows the maximum values of clays and the last one still presents high values of clay but

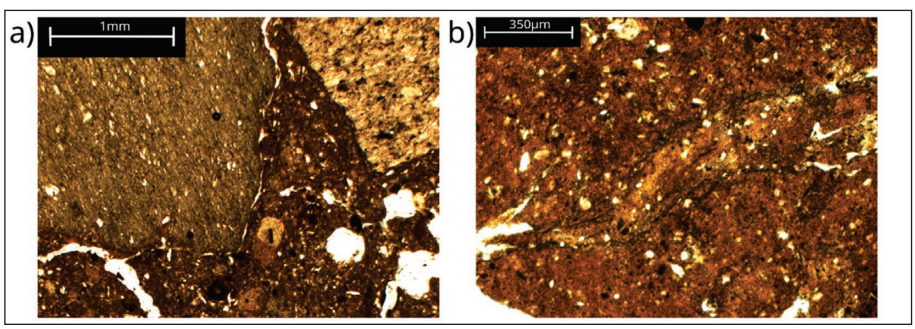

Figure 8: Micromorphology of the diamicton profiles. a) Atl 1-Level 1. Rock fragments in a brown matrix with other materials fragments PPL; and b) Atl 2-Level 2. Matrix with fluidal structure PPL. PPL: plane polarized light, NX crossed polarizers.

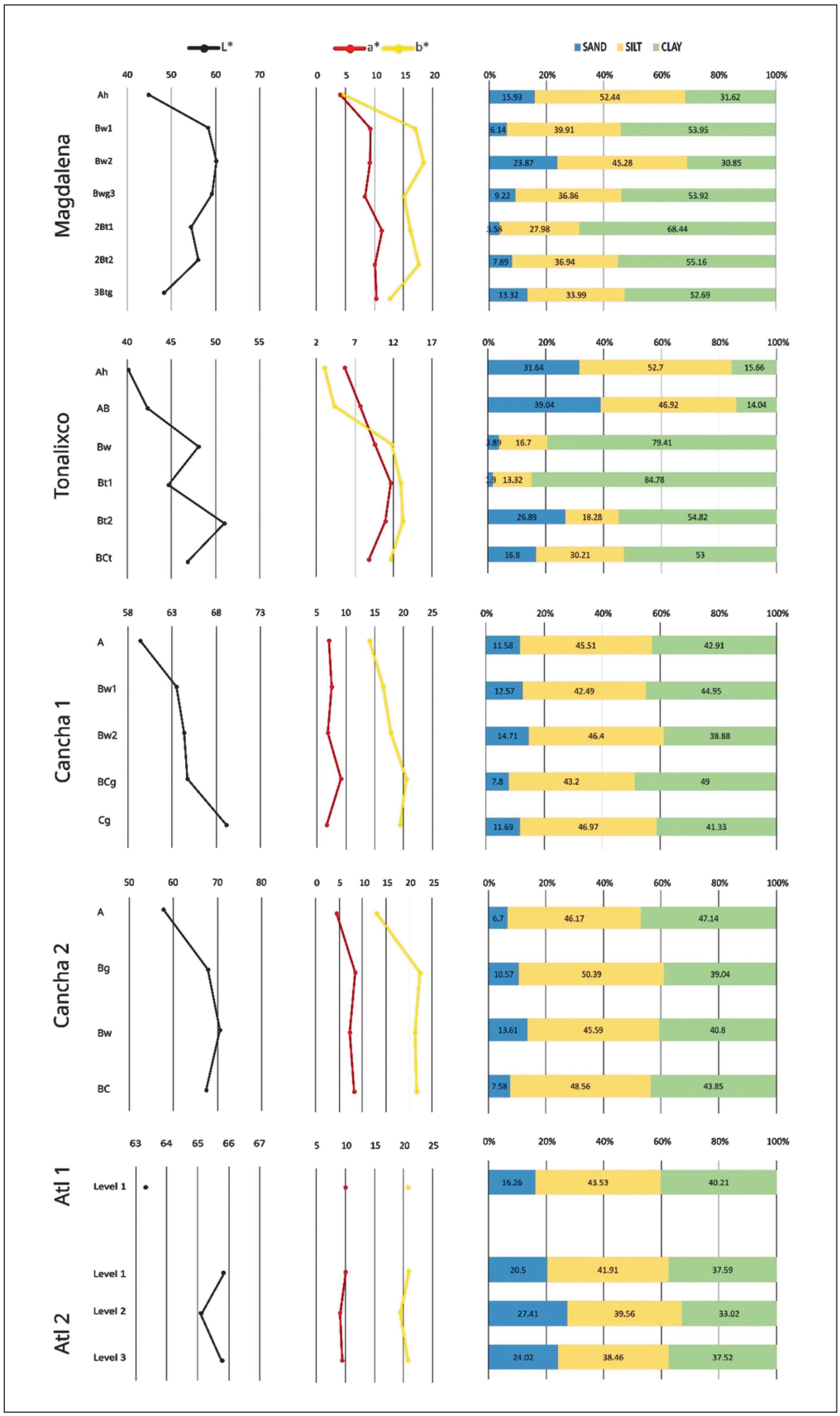

*Figure 9: Physicochemical properties of studied profiles. Colorimetry Lab color (L*a*b*), and Texture.*

with higher values of sand and silt. The texture type is loam in the surface and clay below.

The Stagnosols profiles present silty clay and silty clay loam textures. Both present a homogeneous distribution of percentages through the profile, the difference being a higher amount of sand in the Cancha 1 profile while in the Cancha 2 profile silt predominates.

The Diamicton profiles present a silty clay texture in the Atl 1 profile and a clay-loam texture in the Atl 2 profile. They also show a uniform distribution of size particles, with silt, the predominant one, followed by clay and a higher percentage of sand than in the other groups of profiles.

3.2.4 Mineralogical investigations by X-ray diffractometry (XRD)

Bulk rock samples. One horizon of each profile was analyzed to present the general mineralogical composition (Table 2). The most abundant primary minerals identified were quartz, plagioclase of intermediate composition, and magnetite. Gibbsite-type Al-hydroxides, calcite, and different proportions of 2:1 phyllosilicate (chlorite, vermiculite and illite) and 1:1 phyllosilicates of the kaolinite group were identified as secondary minerals.

As seen in Figure 10a, the Diamicon profiles are quite similar to the Stagnosol profiles, especially regarding the presence of primary minerals and the predominance of 2:1 phyllosilicates. Consequently, they are quite different from the Terra Rossa Type in which secondary minerals, especially kaolinitic clays and gibbsite-type hydroxides, predominate (Figure 10a). The Diamicton profiles are the only ones where calcite was found, while the plagioclase was only found in the Stagnosol profiles. Gibbsite is present only in horizon Bw1 of Magdalena

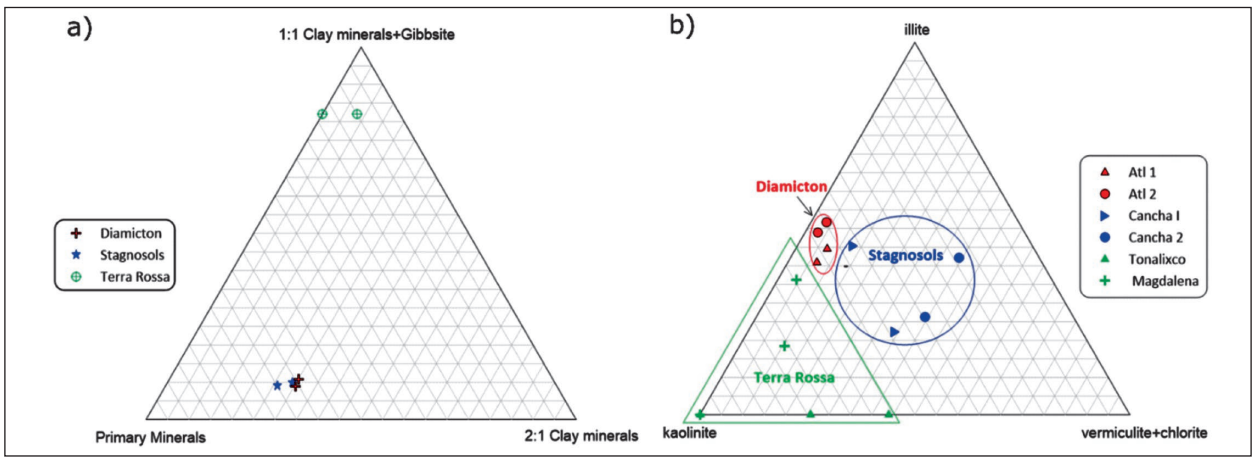

Figure 10: Ternary diagram of Bulk rock and Oriented samples. a) Bulk rock diagram from the RIR Mineralogical semiquantitative percentages. Primary minerals= quartz, plagioclase and magnetite; 2:1= vermiculite, chlorite and ilite phyllosilicates; and 1:1= gibbsite and kaolinite phyllosilicates; and b) Principal clay components from the semi quantitative analysis of the oriented sample.

Table 2: Bulk rock RIR mineralogical semiquantitative percentages. T= Tonalixco, M= Magdalena, C1= Cancha 1, C2= Cancha 2, A1= Atl 1, and A2= Atl 2. The values projected in the ternary diagram (Figure 10) correspond to the last columns of this table. The last 2 rows show the corrected values by removing carbonate in the diamicton profiles.

	Primary Minerals			Oxides		T:O	T:O:T			TOT	TO	Primary
	Pl	Qz	Cc	Mag	Gib	K	il	Cl/Ver		02:01	1:1+Gib	Primary
A1 L1		49	7	6		10	19		100	28	10	62
A2 L2		47	11	7		8	19	8	100	27	8	65
T-Bt1		10				82		8	100	8	82	10
M-BW1		13		5	30	52			100	0	82	18
C2-BC	15	45		5		9	14	12	100	26	9	65
C1-Bw1	6	49		6		10	16	13	100	29	10	61
A1 L1		52.7		6.5		10.8	20.4	9.7	100	30.1	10.8	59.1
A2 L2		52.8		7.9		9.0	21.3	9.0	100	30.3	9.0	60.7

profile (Table 2) and it should be interpreted as the product of intense weathering of aluminosilicate-rich rocks (feldspars or aluminum-rich clays such as kaolinite) under humid tropical and subtropical climate conditions.

Oriented Samples. 14 samples were analyzed considering the clay content and distribution through the profile (Table 3). The primary 2:1 phyllosilicates components identified are Vermiculite and some chlorite at 14Å, as well as Ilite at 10Å; in the 1:1 phyllosilicates kaolinite was identified at 7Å, of this phase, two components were

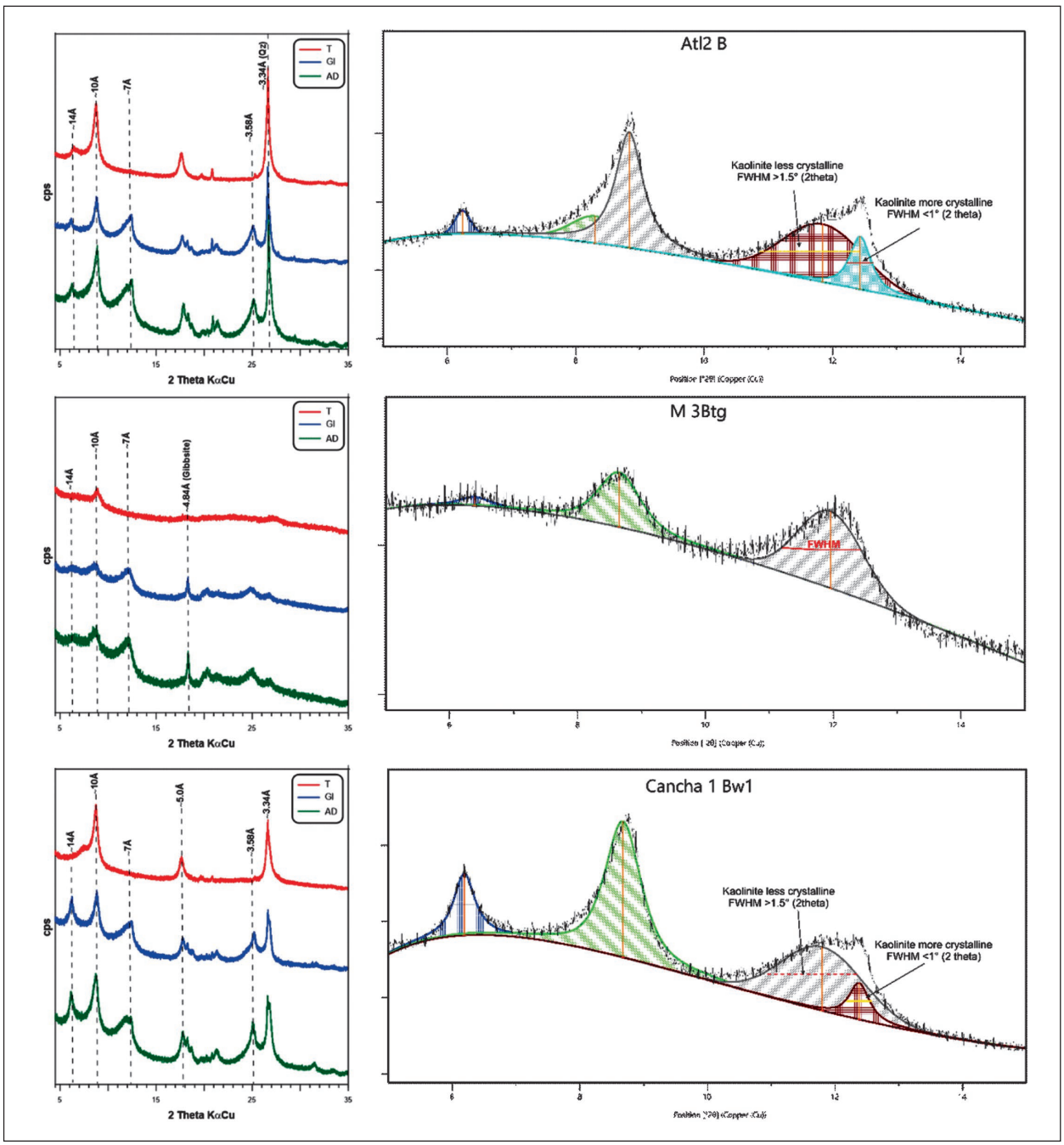

Figure 11: Comparative oriented sample diffractograms and semiquantitative analysis. T = 550°C, Gl = ethylene glycol saturated, and AD = air-dried form. The diffractograms show the peaks of vermiculite and chlorite at 14Å, ilite at 10Å, and kaolinite at 7Å, as well as gibbsite at 4.84Å, and quartz at 3.34Å. In the semiquantitative diagrams, profile fitting of the peak located at approximately 7Å for samples Atl 2 Level B and Cancha 1 BW1 required two components with different FWHM values. In contrast, only a single component was identified in sample M 3Btg. This indicates the possible coexistence of two types of kaolinite, with different crystallinity (FWHM values).

Table 3: Oriented sample semiquantitative weight percentages. T= Tonalixco, M= Magdalena, C1= Cancha 1, C2= Cancha 2, A1= Atl 1, and A2= Atl 2. AD: air-dried form, GL: ethylene glycol saturated, T: 550°C, (): Peaks not clearly defined, ?: undifferentiated, X: collapse peak.

SAMPLE	AD	GL	T	PHASE	% (weight)
T-AB	~14Å	~14Å	~12Å	Vermiculite	26.4
	~10Å	~10Å	~10Å	illite	40.0
	~7Å	~7Å	X	Kaolinite	33.7
T-Bt1	~13Å	**?**	~10	*Mixed layered vermiculite-illite*	13.1
	~10Å	~10Å	~10Å	illite	49.1
	~7Å	~7Å	X	*Kaolinite*	37.8
T-BCt	~12Å	**?**	~10Å	*Mixed Layer vermiculite-illite*	19.4
	~10Å	~10Å	~10Å	illite	33.3
	~7Å	~7Å	X	Kaolinite	47.2
M-BW1	~10Å	**?**	~10Å	illite	61.3
	~7Å	~7Å	X	Kaolinite	38.7
M-2Bt1	~10Å	**?**	~10Å	illite	18.3
	~7Å	~7Å	~7Å	Kaolinite	71.1
M-3Btg	~13-14Å	**?**	~12Å	Vermiculite	4.4
	~10Å	**?**	~10Å	illite	36.1
	~7Å	~7Å	X	Kaolinite	59.5
C2-A	~13Å	~13Å	~13Å	*Mixed layered illite-chlorite*	39.2
	~10Å	~10Å	~10Å	illite	26.2
	~7Å	~7Å	X	Kaolinite 1	24.3
	~7Å	(~7Å)	(X)	Kaolinite 2	10.3
C2-BC	~14Å	~13-14Å	~12Å	Vermiculite	39.3
	~10Å	~10Å	~10Å	illlite	42.2
	~7Å	~7Å	X	Kaolinite	18.6
C1-Bw1	~14Å	~13-14 Å	~11-12Å	Vermiculite	13.0
	~10Å	~10Å	~10Å	illite	45.4
	~7Å	~7Å	X	Kaolinite 1	7.2
	~7Å	(~7Å)	(X)	Kaolinite 2	34.4
C1-BCg	~14Å	~13Å	~11-12Å	Vermiculite	34.2
	~10Å	~10Å	~10Å	illite	22.3
	~7Å	~7Å	X	Kaolinite	43.5
A1 L1	~14Å	~13-14Å	~12Å	Vermiculite	6.8
	~10Å	~10Å	~10Å	illite	40.9
	~7Å	~7Å	X	Kaolinite 1	16.1
	~7Å	(~7)Å	(X)	Kaolinite 2	36.2
A2 L1	~14Å	~13-14Å	~12Å	Vermiculite	7.4
	~9-10Å	~10Å	~10Å	illite	44.5
	~7Å	~7Å	X	Kaolinite 1	30.0
	~7Å	?	X	Kaolinite 2	18.1
A2 L2	~14Å	~14Å	~12-13Å	Vermiculite	2.9
	10Å	9Å	10Å	illite	49.0
	7Å	7Å	X	Kaolinite 1	12.2
	7Å	(7)Å	(X)	Kaolinite 2	35.9
A2 L3	14Å	13Å	13Å	Mixed layered vermiculite-chlorite	3.6
	9Å	9Å	10Å	illite	51.7
	7Å	7Å	X	Kaolinite 1	11.1
	7Å	(7)Å	(X)	Kaolinite 2	33.6

identified in the Stagnosols and Diamicton groups, one with better crystallinity than the other as seen through its FWHM (Full Width at Half Maximum) values (Figure 11).

Figure 10b shows how the proportions of these phases differentiate the soil groups. The surface soils present different proportions of these components, the predominant phase in the Terra Rossa Type profiles is kaolinite, followed by illite and minor content of vermiculite, in the Magdalena profile there is also presence of gibbsite. On the other hand, the Stagnosols profiles present similar proportions of the different components, the 2:1 clay is present in higher quantities like the illite and kaolinite, the latter component presents two phases, one with low crystallinity (FWHM values of <1.5 (2 theta)) and one with higher crystallinity (FWHM values of <1° (2 theta)). The Diamicton, are like the soils of the Stagnosols group, with higher content of illite, two kaolinite components and the presence of a 2:1 clay that is chlorite.

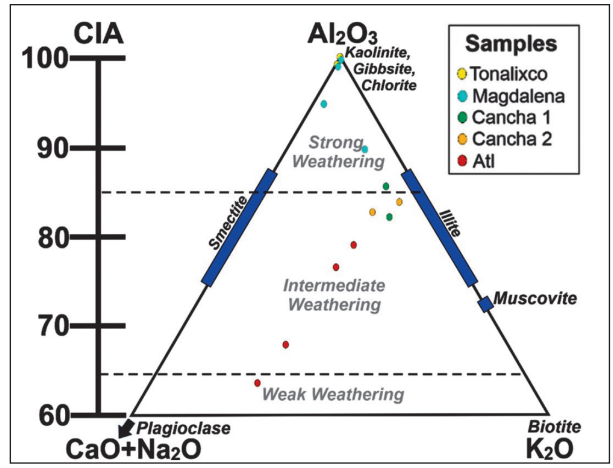

Figure 12: Chemical Index of Alteration (CIA) ternary plot of molecular proportions Al_2O_3-(CaO + Na_2O)-K_2O showing the weathering trend of the studied materials after Nesbitt and Young (1982) and Fedo et al. (1995).*

3.2.5 Bulk chemical composition by X-Ray Fluorescence (XRF)

For 15 samples analyzed, we calculated the Chemical Index of Alteration (CIA) and built a ternary plot of molecular proportions Al_2O_3-(CaO* + Na_2O)-K_2O, for establishing interrelations between different soil and sediment materials (Figure 12, Table 4). In this plot the grouping of the Terra Rossa Type profiles in the superior triangle corner is visible, where an extreme accumulation of secondary minerals, such as kaolinite and gibbsite, was encountered; the same profiles show the highest values of CIA in contrast the Diamicton and the Stagnosols profiles are associated with an intermediate weathering; the latter group is associated with a trend of illite accumulation.

Table 4: XRF elemental analysis of major elements. T= Tonalixco, M= Magdalena, C1= Cancha 1, C2= Cancha 2, A1= Atl 1, and A2= Atl 2.

	SiO2%	TiO2%	Al2O3%	Fe2O3t%	MnO%	MgO%	CaO%	Na2O%	K2O%	P2O5%	PXC%
Profile horizon	wt	wt	wt	wt	wt	wt	wt	wt	wt	wt	wt
T-AB	32.192	1.912	29.817	12.272	0.079	0.65	0.339	0.086	0.111	0.223	22.32
T-Bt1	37.634	1.689	32.362	12.342	0.022	0.406	0.05	0.002	0.242	0.143	15.11
T-BCt	37.573	1.66	32.676	12.323	0.043	0.322	0.185	0.002	0.178	0.3	14.74
M-Ah	24.142	1.482	30.439	10.739	0.07	0.492	0.889	0.167	0.313	0.217	31.05
M-Bw1	34.321	1.513	35.295	11.438	0.019	0.17	0.209	0.002	0.051	0.043	16.94
M-2Bt1	17.209	1.943	41.891	14.687	0.021	0.268	0.083	0.002	0.117	0.042	23.74
M-3Btg	40.392	1.599	28.576	11.198	0.182	1.052	0.526	0.002	2.248	0.027	14.2
C1-Bw1	59.314	0.89	18.812	6.908	0.146	1.729	0.243	0.442	2.91	0.095	8.51
C1-Cg	62.621	0.994	17.744	5.892	0.039	1.376	0.315	0.071	2.249	0.047	8.65
C2-Ah	59.869	1.051	15.718	5.718	0.069	1.557	0.519	0.188	2.077	0.085	13.15
C2-BC	57.583	0.935	19.34	7.643	0.086	1.887	0.277	0.082	2.984	0.042	9.14
A1-Level 1	56.853	1.002	19.568	7.009	0.128	1.353	1.939	0.047	2.682	0.209	9.21
A2-Level 1	58.92	0.956	19.038	6.827	0.123	1.301	1.425	0.148	2.634	0.257	8.37
A2-Level 2	54.71	0.894	18.019	6.38	0.126	1.364	4.751	0.118	2.653	0.594	10.39
A2-Level 3	54.234	0.913	18.65	6.764	0.118	1.426	4.079	0.076	2.721	0.7	10.32

4. DISCUSSION

4.1 KARSTIC SETTING

Atl Cave is developed in the Sierra Zongolica. Its surface geomorphology exhibits many mountains and hills alternating with closed karst depressions such as poljes and dolines, additionally karstic pockets and criptodolines are widely distributed (Hernández-Vergara, 2017), all of this resulted from the deformation of Mesozoic rocks by different events of uplifted, shortened and transported northeastward forming a fold and thrust belt during the Laramide orogeny (Eguiluz et al., 2000; Ortuño-Arzate et al., 2003).

Atl Cave is a high relief multilevel structure considered as an epigenetic cave with a point recharge zone at the entrance fed by a water stream, which is part of the drainage system in the basin of Tecolayo Mountain. Sediments are mainly represented by a thick diamicton facies that have filled the conduits in the past; however, these sediments are currently eroded by the stream. The evolution of Atl Cave can be divided into the following stages:

Conduits development. The cave started to form in the first stage of karstification, following the model of Dreybrodt and Gabrovšek (2003) suggesting that these morphologies are initiated in areas with intense rainfall, when the discharge within the karst system exceeds the capacity of its conduits. Favoring the dissolution-erosive process and conduit development in the upper part of valleys, while depositional processes prevail in the lower part of valleys linked to the water table (Dreybrodt and Gabrovšek, 2003; Audra and Palmer, 2015). This denotes that development of conduits in Atl cave is linked to ancient tectonic events such as stability (phreatic conduits) and uplift (vadose conduits) which were developed previously to the arrival of diamicton facies.

Cave filling. As discussed in the next section, the diamicton facies inside the cave correlate with the facies in the Stagnosols soil profiles filling the doline partially and the cave almost entirely. This is corroborated by the observation of some vadose conduits completely filling and in some sections a residue of diamicton in the conduit ceilings has remained. This type of facies is related to extreme floods, frequently associated with catastrophic floods and glacial melt events (Bosch and White, 2007, 2018). In Atl cave, the sediments could be associated with debris flows originated in landslides and other catastrophic events during high precipitation seasons.

4.2 FORMATION OF THE DEPOSITS INSIDE THE CAVE

The Diamicton group are facies composed of between 30 and 50% poorly consolidated unsorted rock fragments without clear sedimentary structures. Its texture is clay loam and silty clay, and presents the highest percentage of sand particles compared to the surface profiles. The clay mineralogy shows the presence of illite and kaolinite as principal components with some minimal vermiculite and chlorite. Same as the Adjacent to Cave, these profiles present two kaolinite components differentiated by its crystallinity. The mineralogy of these profiles shows the presence of primary minerals as well as Calcite that is interpreted as an input from the cave. These profiles present an intermediate and weak weathering following the Chemical Index of Alteration. Micromorphologically the same fluidal structures as in the Stagnosols profiles can be seen.

The similarities with the Stagnosols profiles, as well as the location of these at the entrance of the cave, indicate the origin of these diamicton facies by the transport of materials from the doline. The absence of sedimentary structures like gradation among others suggests transportation into the cave in a debris flow. This finding is interesting because even when a stream is present in the cave, the studied sediments do not display a clear channel, or fluvial facies expected in this type of cave. Instead, the sediment transport to the cave seems to be related to ground mass or high energy events generating hyper-concentrated fluxes. Similar sediment sequences are common in fluviokarstic drainage basins, such as those shown at Mammoth Cave (Bosh and White, 2007, 2018; Bosch et al., 2021); even within pseudo karstic caves as Karmidas (Aliaga-Campuzano et al., 2017). Contrast with platform karst landscapes, where caves are mainly horizontal with low hydraulic gradients as in the Yucatan Peninsula, where the suffusion process is one of the main mechanisms of fine sediment transport (Sedov et al., 2023).

4.3 PEDOGENESIS OF THE STUDIED PROFILES

In the soil cover outside the cave, two groups were identified: Terra Rosa Type and Stagnosols. These present different pedogenesis in terms of parent material and time, which results in different physicochemical characteristics that are also present within each group.

The Terra Rosa Type profiles correspond to deep reddish Luvisols. The predominant texture is clay and tends to be present in the lower horizons. The princi-

pal clay mineralogy component is kaolinite, with some vermiculite. The upper horizons present a higher percentage of sand and silt fractions, which could indicate the contribution of volcanic ash fall material, that could explain the presence of pyroxene and plagioclase. The contribution of long-distance volcanic ash falls could be associated to some activity from the Pico de Orizaba volcano and surrounding areas (Schaaf and Carrasco-Nuñez, 2010). The presence of kaolinite and gibbsite, as well as the general characteristics of the profiles, indicates a longer period of weathering and pedogenesis, as shown in the Chemical Index of Alteration (Figure 12). Only the Magdalena profile presents Gibbsite maybe indicating a longer period of pedogenesis. In subtropical and temperate regions, the presence of gibbsite could be associated to deeper soil horizons with high leaching rates (Macías-Vázquez, 1981; Kämpf et al., 2012; Caner et al., 2014). Gibbsite can form directly from the weathering of primary aluminum-containing minerals, such as plagioclase, however more common is its formation through the long-term progressive desilication of aluminosilicates (Muggler et al., 2007; Gasparini et al., 2024).

The Stagnosol profiles are deep, with around 45% of weathered rocks and redox properties. The predominant texture is silty clay. The clay mineralogy components present are vermiculite, illite and kaolinite in similar semiquantitative percentages. This group presents two types of kaolinite, one more crystalline than the other, according to the different FWHM values. In kaolinite, a low FWHM suggests formation in stable environments under conditions that favor recrystallization, whereas a high FWHM may be linked to rapid neoformation or intense weathering.

The presence of the different clay components suggests a diverse contribution of parent material, probably the apport of eolian volcanic material, and terrigenous sediments from the Necoxtla formation that is present in the upper part of the basin. The mineralogy shows the presence of primary minerals, which considering the CIA values, locates them in an intermediate weathering and pedogenesis. Micromorphologically the Cancha 1 profile presents fluidal structures that are not present in Cancha 2, referring to fluvial processes in its formation.

The development of different soil types seems to be related to their geomorphic position. The Terra Rossa Type are in depression of the relief where accumulation and no clear erosion is possible, while the Adjacent to Cave are in an area of high hydrology flux that drains into the cave, being highly susceptible to lateral erosion. The relevance of allochthonous material for the formation of the soils is evident; the presence of volcanic material in the area has been presented in the form of lahars, pumice and volcanic ash fall in other research (Ferrand et al., 2014; Solleiro et al., 2023).

5. CONCLUSION

Through the study of soil and sediment profiles close to the Atl cave in the Sierra Zongolica Mountain range, we were able to understand the deposition processes of the diamicton facies inside the cave, as well as the pedogenesis of the soil cover around the cave from which the sediments are formed. Three main conclusions are drawn from this study:

- The diamicton deposits inside the cave correspond to high energy events generating hyper-concentrate fluxes from the surface, and not to suffusion of the soils on top of the cave. These events transport materials trapped in the doline outside the cave.
- There is an important input of silicate material for the pedogenesis of the soils in the form of volcanic ash fall probably from the Pico de Orizaba and terrigenous sediments from the Necoxtla formation.
- The pedodiversity of the area is highly related to the relief in which the soils develop. The Terra Rossa Type profiles are on stable depressions that allows for continuous pedogenesis, while the Stagnosols profiles are in a more dynamic position that cuts the pedogenesis and gives colluvial properties to these soils.

The finding of this study helps us to understand the sedimentary dynamics in tropical mountainous karst systems, where lateral processes seem to be the main factor in the formation of these cave sediments. Further study of other caves and sediments can expand our understanding of the processes in this particular geosystem.

ACKNOWLEDGEMENTS

This work was supported by the PAPIIT proyect IN105819 in the UNAM (Sergey Sedov). We are grateful to the Secretaria de Ciencia, Humanidades, Tecnología e Innovación (SECIHTI) for the scholaship to Pamela García during her postgraduate studies. Many thanks

to Jaime Díaz Ortega for the manufacture of thin sections in the Taller de Suelos y Sedimentos in Intituto de Geología UNAM, as well to the Laboratorio de Difracción de Rayos X (Teresa Pi) of the Laboratorio Nacional de Gequímica y Mineralogía (LANGEM-UNAM) and Laboratorio de Fluorescencia de Rayos X (Rufino Lozano and Patricia Girón) of the Laboratorio Nacional de Geoquímica y Mineralogía (LANGEM-UNAM)..

REFERENCES

Aliaga-Campuzano, M. D. P., López-Martínez, R., Dávila-Harris, P., Espinasa-Pereña, R., Espino del Castillo, A., Bernal, J.P., 2017. Timing of speleogenesis of Las Karmidas Cave (Mexico): First description of pseudokarst developed in ignimbrite. International Journal of Speleology, 46(3): 331–343. https://doi.org/10.5038/1827-806X.46.3.2097

Ardelean, C.F., Becerra-Valdivia, L., Pedersen, M.W., Schwenninger, J.L., Oviatt, C.G., Macías-Quintero, J.I., Arroyo-Cabrales, J., Sikora, M., Ocampo-Díaz, Y.Z.E., Rubio-Cisneros, I.I., Watling, J.G., De Medeiros, V.B., De Oliveira, P.E., Barba-Pingarrón, L., Ortiz-Butrón, A., Blancas-Vázquez, J., Rivera-González, I., Solís-Rosales, C., Rodríguez-Ceja, M., Gandy, D.A., Navarro-Gutiérrez, Z., De La Rosa-Díaz, J.J., Huerta-Arellano, V., Marroquín-Fernández, M.B., Martínez-Rojas, L.M., López-Jiménez, A., Higham, T., Willerslev, E., 2020. Evidence of human occupation in Mexico around the Last Glacial Maximum. Nature, 584: 87–92. https://doi.org/10.1038/s41586-020-2509-0

Atalay, I., 1997. Red Mediterranean soils in some karstic regions of taurus mountains, Turkey. CATENA, 28(3): 247–260. https://doi.org/10.1016/S0341-8162(96)00041-0

Audra, P., Palmer, A.N., 2015. Research frontiers in speleogenesis. Dominant processes, hydrogeological conditions and resulting cave patterns. Acta Carsologica, 44(3): 315-348 https://doi.org/10.3986/ac.v44i3.1960

Bautista, F., Palacio-Aponte, G., Quintana, P., Zinck, J.A., 2011. Spatial distribution and development of soils in tropical karst areas from the Peninsula of Yucatan, Mexico. Geomorphology, 135(3): 308–321. https://doi.org/10.1016/j.geomorph.2011.02.014

Beach, T., Dunning, N., Luzzadder-Beach, S., Cook, D. E., Lohse, J., 2006. Impacts of the ancient Maya on soils and soil erosion in the central Maya Lowlands. CATENA, 65(2): 166–178. https://doi.org/10.1016/j.catena.2005.11.007

Beck, B., 2012. Soil Piping and Sinkhole Failures. In: White, W.B., Culver, D.C. (Eds.), Encyclopedia of Caves. Academic Press, Oxford. pp. 718–723.. https://doi.org/10.1016/B978-0-12-383832-2.00106-7

Béres, S., Cserpák, F., Moskal-del Hoyo, M., Repiszky, T., Sázelová, S., Wilczyński, J., Lengyel, G., 2021. Zöld Cave and the Late Epigravettian in Eastern Central Europe. Quaternary International, 587–588: 158–171. https://doi.org/10.1016/j.quaint.2020.09.050

Bosch, R.F., White, W.B., 2007. Lithofacies and transport of clastic sediments In: Sasowsky, I.D., Mylroie, J. (Eds.), Studies of Cave Sediments. Physical and Chemical Records of Paleoclimate, Springer, Dordrecht, pp. 1–22 https://doi.org/10.1007/978-1-4020-5766-3_1

Bosch, R.F., White, W.B.,2018. Lithofacies and Transport for Clastic Sediments in Karst Conduits. In: White, W.B., Herman, J.S., Herman, E.K., Rutigliano, M. (Eds.), Karst Groundwater Contamination and Public Health, Springer International Publishing, Dordrech, pp. 277–281. https://doi.org/10.1007/978-3-319-51070-5_32

Bosch, R., Ward, D., Bird, A., Sturmer, D., Olson, R.,2021. A debris flow deposit in Mammoth Cave: Field characterization. Journal of Cave and Karst Studies, 83(4): 151–162. https://doi.org/10.4311/2020ES0108

Bronger, A., Sedov, S.N., 2003. Vetusols and paleosols: Natural versus man-induced environmental change in the Atlantic coastal region of Morocco. Quaternary International, 106–107: 33–60. https://doi.org/10.1016/S1040-6182(02)00160-X

Burger, P.A., 2004. Glacially-Influenced Sediment Cycles in the Lime Creek Karst, Eagle County, Colorado. In: Sasowsky, I.D., Mylroie, J. (Eds.), Studies of Cave Sediments. Springer, Dordrecht, pp. 107–122. https://doi.org/10.1007/978-1-4419-9118-8_7

Cabadas-Báez, H., Solleiro-Rebolledo, E., Sedov, S., Pi-Puig, T., Gama-Castro, J., 2010. Pedosediments of karstic sinkholes in the eolianites of NE Yucatán: A record of Late Quaternary soil development, geomorphic processes and landscape stability. Geomorphology, 122(3): 323–337. https://doi.org/10.1016/j.geomorph.2010.03.002

Caner, L., Radtke, L.M., Vignol-Lelarge, M.L., Inda,

A.V., Bortoluzzi, E.C., Mexias, A.S., 2014. Basalt and rhyo-dacite weathering and soil clay formation under subtropical climate in southern Brazil. Geoderma, 235–236: 100–112. https://doi.org/10.1016/j.geoderma.2014.06.024

Carrasco-Núñez, G.,1999. Holocene block-and-ash flows from summit dome activity of Citlaltépetl volcano, Eastern Mexico. Journal of Volcanology and Geothermal Research, 88(1–2): 47–66. https://doi.org/10.1016/S0377-0273(98)00110-3

Carrasco-Núñez, G., Rose, W.I., 1995. Eruption of a major Holocene pyroclastic flow at Citlaltépetl volcano (Pico de Orizaba), México, 8.5–9.0 ka. Journal of Volcanology and Geothermal Research, 69(3–4): 197–215. https://doi.org/10.1016/0377-0273(95)00023-2

Dreybrodt, W., 2019. Speleothem deposition. In: White, W.B., Culver, D.C., Pipan, T. (Eds.), Encyclopedia of Caves. Academic Press, UK., pp. 996–1005. https://doi.org/10.1016/B978-0-12-814124-3.00116-3

Dreybrodt, W., Gabrovšek, F., 2003. Basic Processes and Mechanisms Governing the Evolution of Karst. KIP Research Publications at Digital Commons University of South Florida, Articles, 4792.
https://digitalcommons.usf.edu/kip_articles/4792

Dunning, N.P., Luzzadder-Beach, S., Beach, T., Jones, J.G., Scarborough, V., Culbert, T.P., 2002. Arising from the Bajos: The Evolution of a Neotropical Landscape and the Rise of Maya Civilization. Annals of the Association of American Geographers, 92(2): 267–283. https://doi.org/10.1111/1467-8306.00290

Durn, G., 2003. Terra Rossa in the Mediterranean Region: Parent Materials, Composition and Origin. Geologia Croatica, 56(1): 83–100. https://doi.org/10.4154/GC.2003.06

Durn, G., Ottner, F., Slovenec, D., 1999. Mineralogical and geochemical indicators of the polygenetic nature of terra rossa in Istria, Croatia. Geoderma, 91(1): 125–150. https://doi.org/10.1016/S0016-7061(98)00130-X

Eguiluz De Antuñano, S., Aranda García, M., Marrett, R., 2000. Tectónica de la Sierra Madre Oriental, México. Boletín de la Sociedad Geológica Mexicana, 53(1): 1–26. https://doi.org/10.18268/BSGM2000v53n1a1

Fedo, C.M., Wayne Nesbitt, H., Young, G.M., 1995. Unraveling the effects of potassium metasomatism in sedimentary rocks and paleosols, with implications for paleoweathering conditions and provenance. Geology, 23(10): 921-924. https://doi.org/10.1130/0091-7613(1995)023<0921:UTEOPM>2.3.CO;2

Ferrand, P.A., Solleiro-Rebolledo, E., Acosta, G., Sedov, S., Morales, P., 2014. Archaic settlement in El Tebernal, Veracruz: First insights into paleoenvironmental conditions and resource exploitation. Quaternary International, 342: 45–56. https://doi.org/10.1016/j.quaint.2013.12.038

Ford, D.C., Williams, P., 2007. Karst Hydrogeology and Geomorphology. John Wiley & Sons, Chichester, 562 pp. . https://doi.org/10.1002/9781118684986

Gasparini, A.S., Fontes, M.P.F., Pacheco, A.A., Ker, J.C., 2022. Gibbsite Crystallinity and Morphology in Ferralsols and Bauxites. Minerals, 12(11): 1441. https://doi.org/10.3390/min12111441

Harmon, R.S., Schwarcz, H.P., Gascoyne, M., Hess, J.W., Ford, D.C., 2007. Paleoclimate Information From Speleothems: The Present As A Guide To The Past. In: Sasowsky, I.D., Mylroie, J. (Eds.), Studies of Cave Sediments. Physical and Chemical Records of Paleoclimate. Springer, Dordrecht, pp. 199–226. https://doi.org/10.1007/978-1-4020-5766-3_11

Hubbard, C.R., Snyder, R.L., 1988. RIR - Measurement and Use in Quantitative XRD. Powder Diffraction, 3(2): 74–77. https://doi.org/10.1017/S0885715600013257

IUSS Working Group WRB 2015. World Reference Base for Soil Resources 2014, update 2015. International soil classification system and creatinfg legendsfor soilmaps. World Soil Resources Reports No. 106. FAO, Rome. 199 pp.

Kämpf, N., Scheinost, A.C., Schulze, D.G., 2012. Oxide Minerals in Soils, In: Huang, P.M., Li, Y., Summer, M.E. (Eds.), Handbook of Soil Sciences. Properties and Processes, Second Edition, CRC Press, London, pp. 24.1-24.34.

Knapp, E.P., Terry, D.O., Harbor, D.J., Thren, R.C., 2007. Reading Virginia's Paleoclimate From The Geochemistry And Sedimentology Of Clastic Cave Sediments. In: Sasowsky, I.D., Mylroie, J. (Eds.), Studies of Cave Sediments, Springer, Dordrecht, pp. 95–106 https://doi.org/10.1007/978-1-4020-5766-3_6

Loop, C.M., 2019. Contamination of cave waters by nonaqueous-phase liquids. In: White, W.B., Culver, D.C., Pipan, T. (Eds.), Encyclopedia of Caves. Academic Press, UK. pp. 326–332. https://doi.org/10.1016/B978-0-12-814124-3.00036-4

Lynch, F.L., Mahler, B.J., Hauwert, N.N., 2007. Provenance Of Suspended Sediment Discharged From A Karst Aquifer Determined By Clay Mineralogy. In: Sasowsky, I.D., Mylroie, J. (Eds.), Studies of Cave Sediments. Physical and Chemical Records of Paleoclimate. Springer, Dordrecht, pp. 83–93. https://doi.org/10.1007/978-1-4020-5766-3_5

Macías-Vázquez, F., 1981. Formation of gibbsite in soils and saprolites of temperate-humid zones. Clay Minerals, 16(1): 43–52. https://doi.org/10.1180/claymin.1981.016.1.03

Mahler, B.J., Personne, J.-C., Lynch, F.L., Van Metre, P.C., 2007. Sediment And Sediment-Associated Contaminant Transport Through Karst. In: Sasowsky; I.D., Mylroie, J. (Eds.), Studies of Cave Sediments. Physical and Chemical Records of Paleoclimate. Springer, Dordrecht,pp. 23–46. https://doi.org/10.1007/978-1-4020-5766-3_2

Maynard, J.B., 1992. Chemistry of Modern Soils as a Guide to Interpreting Precambrian Paleosols. The Journal of Geology, 100(3): 279–289. https://doi.org/10.1086/629632

Moore, D.M., Reynolds, R.C., 1997. X-ray diffraction and the identification and analysis of clay minerals (2. ed). Oxford University Press, Oxford. 400 pp.

Muggler, C.C., Buurman, P., van Doesburg, J.D.J., 2007. Weathering trends and parent material characteristics of polygenetic oxisols from Minas Gerais, Brazil: I. Mineralogy. Geoderma, 138(1): 39–48. https://doi.org/10.1016/j.geoderma.2006.10.008

Musgrave, R.J., Webb, J.A., 2004. Palaeomagnetic Analysis of Sediments in The Buchan Caves, Southeastern Australia, Provides a Prelate Pleistocene Date for Landscape and Climate Evolution. In: Sasowsky, I.D., Mylroie, J. (Eds.), Studies of Cave Sediments. Physical and Chemical Records of Paleoclimate. Springer, Dordrecht, pp. 47–69. Springer, Dordrecht.. https://doi.org/10.1007/978-1-4419-9118-8_3

Nesbitt, H.W., Young, G.M., 1982. Early Proterozoic climates and plate motions inferred from major element chemistry of lutites. Nature, 299(5885): 715–717. https://doi.org/10.1038/299715a0

Nesbitt, H.W., Young, G.M., 1989. Formation and Diagenesis of Weathering Profiles. The Journal of Geology, 97(2): 129–147. https://doi.org/10.1086/629290

Ortuño-Arzate, S., Ferket, H., Cacas, M.C., Swennen, R., Roure, F., 2003. Late Cretaceous Carbonate Reservoirs in the Cordoba Platform and Veracruz Basin, Eastern Mexico. In: Bartolini, C., Buffler, R.T.,Blickwede, J.F., The Circum-Gulf of Mexico and the Caribbean: Hydrocarbon habitats, basin formation and plate tectonics. American Association of Petroleum Geologists, Memoir 79, pp. 476-514. AAPG, Tulsa, Oklahoma, USA. https://doi.org/10.1306/M79877C22

Price, J.R., Velbel, M.A., 2003. Chemical weathering indices applied to weathering profiles developed on heterogeneous felsic metamorphic parent rocks. Chemical Geology, 202(3–4): 397–416. https://doi.org/10.1016/j.chemgeo.2002.11.001

Priori, S., Costantini, E.A.C., Capezzuoli, E., Protano, G., Hilgers, A., Sauer, D., Sandrelli, F., 2008. Pedostratigraphy of Terra Rossa and Quaternary geological evolution of a lacustrine limestone plateau in central Italy. Journal of Plant Nutrition and Soil Science, 171(4): 509–523. https://doi.org/10.1002/jpln.200700012

Schaaf, P., Carrasco-Núñez, G., 2010. Geochemical and isotopic profile of Pico de Orizaba (Citlaltépetl) volcano, Mexico: Insights for magma generation processes. Journal of Volcanology and Geothermal Research, 197(1): 108–122. https://doi.org/10.1016/j.jvolgeores.2010.02.016

Sedov, S., Rivera-Uria, M.Y., Ibarra-Arzave, G., García-Ramírez, P., Solleiro-Rebolledo, E., Cabadas-Báez, H.V., Valera-Fernández, D., Díaz-Ortega, J., Guillén-Domínguez, K.A., Moreno-Roso, S.J.J., Fedick, S.L., Leonard, D., Golden, C., Morell-Hart, S., Liendo-Stuardo, R.R., 2023. Soil toposequences, soil erosion, and ancient Maya land use adaptations to pedodiversity in the tropical karstic landscapes of southern Mexico. Frontiers in Earth Science, 11. https://www.frontiersin.org/articles/10.3389/feart.2023.1239301

Sedov, S., Solleiro-Rebolledo, E., Fedick, S.L., Pi-Puig, T., Vallejo-Gómez, E., Flores-Delgadillo, M.L., 2008. Micromorphology of a Soil Catena in Yucatán: Pedogenesis and Geomorphological Processes in a Tropical Karst Landscape. In: Kapur, S., Mermut, A., Stoops, G. (Eds.), New Trends in Soil Micromorphology, Springer, Netherlands, pp. 19–37.. https://doi.org/10.1007/978-3-540-79134-8_3

SGM, 2001. Carta geológica minera Orizaba E14-6 Veracruz, Puebla y Oaxaca Escala 1:250000. Servicio Geológico Mexicano. México.

Solleiro-Rebolledo, E., García-Ramírez, P., Sedov, S., Cabadas-Báez, H., Rivera-Uria, Y., Ibarra-Arzave, G., Pi-Puig, T., 2023. Interaction of geomorphic processes and long-term human impact in the soil evolution: A study case in the tropical area at Veracruz, Mexico. CATENA, 227, 107072. https://doi.org/10.1016/j.catena.2023.107072

Springer, G.S., 2019. Clastic sediments in caves. In: White, W.B., Culver, D.C., Pipan, T. (Eds.), *Encyclopedia of Caves*. Academic Press, UK. pp. 277–284. https://doi.org/10.1016/B978-0-12-814124-3.00031-5

Stoops, G., 2020. Guidelines for Analysis and Description of Soil and Regolith Thin Sections (1st ed.). Soil Science Society of America/Wiley, USA, 240 pp. https://doi.org/10.1002/9780891189763

Vesper, D.J., 2019. Contamination of cave waters by heavy metals. In: White, W.B., Culver, D.C., Pipan, T. (Eds.), Encyclopedia of Caves. Academic Press, UK. pp. 320–325. https://doi.org/10.1016/B978-0-12-814124-3.00035-2

White, W.B., 1988. Geomorphology and hydrology of karst terrains. Oxford University Pess:Oxford, UK. 480 pp.

White, W.B., 2004. Paleoclimate Records from Speleothems in Limestone Caves. In: Sasowsky, I.D. Mylroie, J. (Eds.), Studies of Cave Sediments. Springer, Dordrecht, pp. 135–175. https://doi.org/10.1007/978-1-4419-9118-8_9

Wojdyr, M., 2010. Fityk: A general-purpose peak fitting program. Journal of Applied Crystallography, 43(5–1): 1126–1128. https://doi.org/10.1107/S0021889810030499

Yaalon, D.H., 1997. Soils in the Mediterranean region: What makes them different? CATENA, 28(3): 157–169. https://doi.org/10.1016/S0341-8162(96)00035-5

Zupan Hajna, N., Bosák, P., Pruner, P., Mihevc, A., Hercman, H., Horáček, I., 2020. Karst sediments in Slovenia: Plio-Quaternary multi-proxy records. Quaternary International, 546: 4–19. https://doi.org/10.1016/j.quaint.2019.11.010